

Conductance measurement of spin-orbit coupling in the two-dimensional electron systems with in-plane magnetic field

K. Kolasiński,^{1,2} H. Sellier,² and B. Szafran¹

¹*AGH University of Science and Technology, Faculty of Physics and Applied Computer Science,
al. Mickiewicza 30, 30-059 Kraków, Poland*

²*Institut Néel, CNRS and Université Joseph Fourier,
BP 166, 38042 Grenoble, France*

We consider a possibility of determination of spin-orbit (SO) coupling constants for the two-dimensional electron gas from measurements of electric properties in rotated in-plane magnetic field. Due to the SO coupling the electron backscattering is accompanied by spin precession and spin mixing of the incident and reflected electron waves. The competition of the external and SO-related magnetic fields produces a characteristic conductance dependence on the in-plane magnetic field value and orientation which, in turn, allows for determination of the absolute value of the effective spin-orbit coupling constant as well as the ratio of the Rashba and Dresselhaus SO contributions.

Introduction. Charge carriers in semiconductor devices are subject to spin-orbit (SO) interactions [1] stemming from the anisotropy of the crystal lattice and/or the device structure. The SO interactions translate the carrier motion into an effective magnetic fields which acts on the spin of the carriers giving rise to spin relaxation and dephasing [2–4], spin Hall effects [5–7], formation of topological insulators [8], persistent spin helix states [9–11], Majorana fermions [12]. Moreover, the SO interactions pave the way to spin-active devices, including spin-filters based on quantum point contacts (QPCs) [13] or spin transistors [14–18], which exploit the precession of the electron spin in the SO effective magnetic field [19]. The most popular playground for studies of spin effects and construction of spin-active devices is the two-dimensional electron gas (2DEG) confined at the interfaces of an asymmetrically doped III-V heterostructure, with a strong built-in electric fields in the confinement layer giving rise to the Rashba SO coupling [20] and with the Dresselhaus coupling due to the anisotropy of the lattice which is enhanced by a strong localization of the electron gas in the growth direction [21].

The strength of SO interaction is sample-dependent and its characterization is of a fundamental importance for description of spin-related phenomena and design of spin devices. The SO coupling constant are usually derived from the Shubnikov-de Haas [22–29] oscillations, antilocalization of the magnetotransport [30], photocurrents [31], or precession of optically polarized electron spins as a function of their drift momentum [32]. Usually both the Rashba and Dresselhaus interactions contribute to the overall SO coupling. The separation the contributions of both types of SO coupling is challenging and requires optical procedures for spin polarization [31] or time-resolved readout of the effects of the spin precession in the effective SO magnetic field [32]. In this Letter we investigate the possibility for extraction of the Rashba and Dresselhaus SO interactions from the two-terminal conductance. The proposed method does not involve ap-

plication of optical excitation [31, 32] or a particularly complex gating of the system [32]. The procedure given below requires rotation of the sample in an external in-plane magnetic field, which is straightforward as compared to application of the rotated electric field to the sample [32]. Also, the present approach is suitable for high mobility samples and goes without analysis of the localization effects in the magnetotransport [30].

The procedure which is proposed below bases on an idea that the effects of the SO coupling related to the wave vector component in the direction of the current flow can be excluded by a properly oriented external in-plane magnetic field. The procedure requires electron backscattering effects – due to intentionally introduced potentials – or simply to intrinsic imperfections within the sample. In particular we show that the linear conductance of a disordered sample reveals an oscillatory behavior as a function of the magnetic field direction and amplitude. The dependence of conductance on \mathbf{B} vector direction and length allows one to determine the strength of the SO interaction as compared to the spin Zeeman effect as well as the relative strength of both Rashba and Dresselhaus contributions.

Spin-dependent scattering model. Let us start from a simple model of electron scattering (see Fig. 1) in presence of SO interaction in a system with an impurity. The incident Fermi-level electron spatial wave function – described by a plane wave e^{ikr} – comes to the impurity from the left-hand side and is backscattered. For the discussion we assume that the impurity is hard so that the electron is backscattered with probability 1. We describe the spin states of the incident and backscattered wave by $|k_{\sigma}^{\pm}\rangle$ where k_{σ}^{\pm} denotes the absolute value of the wave vector for the spin state σ and the sign in the superscript indicates the electron incoming from left + or backscattered by the impurity –. The scattering wave function can be then written in terms of the available transport modes

$$|\Psi_{\sigma}\rangle = e^{ik_{\sigma}^{+}r} |k_{\sigma}^{+}\rangle + \sum_{\sigma'} a_{\sigma\sigma'} e^{-ik_{\sigma'}^{-}r} |k_{\sigma'}^{-}\rangle, \quad (1)$$

where $a_{\sigma\sigma'}$ stand for the scattering amplitudes. The

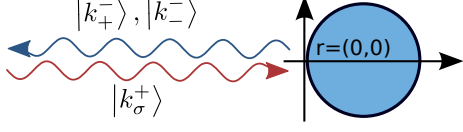


Figure 1. Sketch of considered scattering process. The electron wave is incoming from the left in one of two spin states, propagates to the right and is backscattered at position $r = (0,0)$ by the potential barrier induced by the impurity. Here we assume a hard wall potential profile (i.e. $V_{\text{tip}} = +\infty$ inside the circle).

scattering occurs between the eigenstates of the two-dimensional Hamiltonian

$$H = E_{\text{kin}}\mathbf{I} + \sigma_x(\alpha k_y - \beta k_x + b_x) + \sigma_y(\beta k_y - \alpha k_x + b_y), \quad (2)$$

where $\sigma_{x/y}$ are the Pauli matrices, $E_{\text{kin}} = \frac{\hbar^2 \mathbf{k}^2}{2m_{\text{eff}}}$, m_{eff} is the electron effective mass, α and β are two-dimensional linear SO coupling constants, and finally the spin Zeeman effect for the in-plane magnetic field $\mathbf{B} = (B_x, B_y)$ is introduced by $b_{x/y} = \frac{1}{2}g\mu_B B_{x/y}$. The Zeeman energy will be denoted below by $E_B = \frac{1}{2}g\mu_B |\mathbf{B}| = \sqrt{b_x^2 + b_y^2}$.

Let us first neglect the Dresselhaus coupling ($\beta = 0$). Plane wave solution for the eigenvalues of the Schrödinger equation gives

$$E_{\sigma} = \frac{\hbar^2 \mathbf{k}^2}{2m_{\text{eff}}} + \sigma |\mathbf{p}|, \quad (3)$$

with $\sigma = \{+, -\}$ denoting projections of the spin on the direction of polarization $\mathbf{p} = (\alpha k_y + b_x, -\alpha k_x + b_y)$, and eigenvectors

$$|k_{\sigma}^{\pm}\rangle = \frac{1}{\sqrt{2}} \begin{pmatrix} 1 \\ \sigma \frac{p_x^{\pm} + ip_y^{\pm}}{p^{\pm}} \end{pmatrix} \equiv \frac{1}{\sqrt{2}} \begin{pmatrix} 1 \\ \sigma e^{i\phi(\mathbf{k}_{\sigma}^{\pm}, \mathbf{B})} \end{pmatrix}, \quad (4)$$

for the incident (+) and backscattered (−) directions of the electron motion with $p^{\pm} = |\mathbf{p}^{\pm}|$. Due to the assumed infinite potential generated by the impurity, the scattering wave function in Eq. (1) has to vanish at $r = 0$ (see Fig. 1), $\Psi_{\sigma}(r = 0) = |k_{\sigma}^{+}\rangle + \sum_{\sigma'} a_{\sigma\sigma'} |k_{\sigma'}^{-}\rangle = 0$. By substituting Eq. (4) to this equation one evaluates the scattering amplitudes as

$$a_{\sigma\sigma'} = -\sigma' \frac{\sigma e^{i\phi(\mathbf{k}_{\sigma}^{+}, \mathbf{B})} + \sigma' e^{i\phi(\mathbf{k}_{\sigma'}^{-}, \mathbf{B})}}{e^{i\phi(\mathbf{k}_{\sigma}^{+}, \mathbf{B})} + e^{i\phi(\mathbf{k}_{\sigma'}^{-}, \mathbf{B})}}. \quad (5)$$

In the following we use the material constant for $\text{In}_{0.5}\text{Ga}_{0.5}\text{As}$ alloy with $m = 0.0465m_0$ and the Landé factor $g = 9$, and the Fermi energy $E_F = 20\text{meV}$. For the bulk Rashba [33] constant $\alpha_{3D} = 57.2 \text{ \AA}^2$, the two-dimensional value is $\alpha = \alpha_{3D} F_z$, where F_z is the electric field in the growth-direction. The Rashba constant can be controlled by the external voltages [22] and for

$\text{In}_{0.5}\text{Ga}_{0.5}\text{As}$ SO coupling constants of the order of 5 to 10 meV nm [22] were recorded.

In Fig. 2(a) we present the scattering amplitudes $a_{\sigma\sigma'}$ obtained from Eq. (5) as a function of the direction of the magnetic field $\mathbf{B} = (B \cos(\theta), B \sin(\theta))$, with $B = 5\text{T}$ for scattering direction along the x direction, $\mathbf{k} = (k_x, 0)$. Note that for the magnetic field oriented in the y direction $\theta = \pi/2$ (i.e. for $B = (0, B_y)$) the diagonal elements of the scattering amplitudes are zero. This is a special case for which the spinor in Eq. (4) can be written in the following form $|k_{\sigma}^{\pm}\rangle = \begin{pmatrix} 1 \\ i\sigma d_{\pm} \end{pmatrix}$,

where $d_{\pm} = \text{sign}(-\alpha k_x^{\pm} + b_y)$. For a weak magnetic field $|\alpha k_x^{\pm}| > |b_y|$, we get $d_{\pm} = \mp$, and the orthogonality relation $\langle k_{\sigma'}^d | k_{\sigma}^d \rangle = \frac{1}{2}(1 + \sigma\sigma' dd')$, gives zero for the backscattering to the same spin state $\langle k_{\sigma}^{-} | k_{\sigma}^{+} \rangle = 0$ [see Fig. 2(a)]. On the other hand for high magnetic field $|\alpha k_x^{\pm}| < |b_y|$, and we get $d_{\pm} = 1$, and the spin is conserved $\langle k_{\sigma}^{-} | k_{\sigma}^{+} \rangle = 1$.

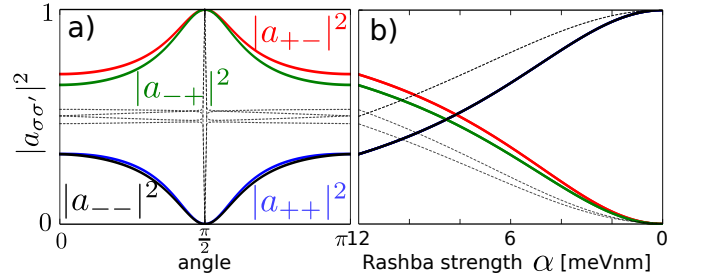


Figure 2. a) Scattering amplitudes calculated from Eq. (5) for $\alpha = 12\text{meVnm}$ and $\beta = 0$ as a function of angle formed by the magnetic field vector and the x axis θ for $B = 5\text{T}$ and electron motion along the x axis. b) Same as in (a), but for a fixed angle $\theta = \pi$ for varying value of Rashba constant α . Black dashed lines show the result for $B = 7.2\text{T}$.

In Fig. 2(b) we show the evolution of the scattering amplitudes for the orientation of magnetic field fixed at $\theta = \pi$, as a function of the Rashba SO constant α . In Eq. (2) we have then $k_y = 0$ and $b_y = 0$. We can see in Fig. 2(b) that the scattering amplitudes cross near $\alpha \approx 8\text{meVnm}$. In this point the Zeeman energy E_B is equal to the SO coupling energy $E_{SO} = \alpha k_x$. In general, we find that for $\alpha k_x = E_B$ the off-diagonal terms can be approximated with $-b_x \sigma_x + (E_B + b_y) \sigma_y$, for which scattering amplitudes (5) for eigenvectors (4) simplify to $|a_{\sigma\sigma'}|^2 = \frac{1}{2}$ for any $\sigma\sigma'$ and for any in-plane vector \mathbf{B} . This case is presented Figs. 2 where the black dashed lines show the scattering amplitudes for $B = 7.2\text{T}$ and $\alpha = 12\text{meVnm}$, i.e. when $E_B \approx E_{SO}$.

Let us now include the Dresselhaus SO coupling. The two-dimensional Dresselhaus constant is given by $\beta = \beta_{3D} \langle k_z^2 \rangle = \beta_{3D} \frac{\pi^2}{d^2}$, where β_{3D} is the bulk constant and d is the width of the two-dimensional gas confinement in the growth direction. We consider β values from 0 to $\simeq \alpha$ [9, 10]. The cubic Dresselhaus interaction is

neglected as a small effect [10]. In the absence of the external field ($b_x = b_y = 0$), for the electron incident along the x direction i.e. $k_y = 0$, the polarization direction is $\mathbf{p} = (-\beta k_x, -\alpha k_x)$ with the energy eigenvalues $E_\sigma = \frac{\hbar^2 k_x^2}{2m_{\text{eff}}} + \sigma k_x \sqrt{\alpha^2 + \beta^2}$. As a result the Dresselhaus interaction sets the direction of the electron spin polarization to $\theta = \arctan\left(\frac{\alpha}{\beta}\right)$ and increases the effective SO coupling constant to $\gamma_{\text{eff}} = \sqrt{\alpha^2 + \beta^2}$.

These conclusions can also be reached by the direct inspection of the off-diagonal part of Hamiltonian (2) for the electron transport along the x direction ($k_y = 0$). The effective magnetic field in Eq. (2) is $(-\beta k_x + b_x, -\alpha k_x + b_y)$. Both components of the effective magnetic field vanish for $\frac{b_y}{b_x} = \frac{\alpha}{\beta}$ and $E_B = \frac{1}{2}g\mu_B B = \sqrt{b_x^2 + b_y^2} = k_x \sqrt{\beta^2 + \alpha^2} = k_x \gamma_{\text{eff}} \equiv E_{SO}$.

For illustration we have considered an electron source at left of the impurity and calculated the electron density at the source position – including the incident and backscattered waves using Eq. (1) as $\rho = \sum_\sigma \langle \Psi_\sigma | \Psi_\sigma \rangle$. For systems with a single perturbation the conductance variation is roughly proportional to the electron density [34]. The electron density – an approximation to the conductance variation – is depicted in Fig. 3 for (a) $\alpha = 12\text{meVnm}$, $\beta = 0$; and (b-c) $\alpha = 9\text{meVnm}$, $\beta = 8\text{meVnm}$. The values adopted in (a,b-c) produce the same value of the effective coupling constant $\gamma_{\text{eff}} \approx 12\text{meVnm}$. The electron source is located in $(-1500\text{nm}, 0\text{nm})$ (a,b) or in $(-2000\text{nm}, 0\text{nm})$ (c).

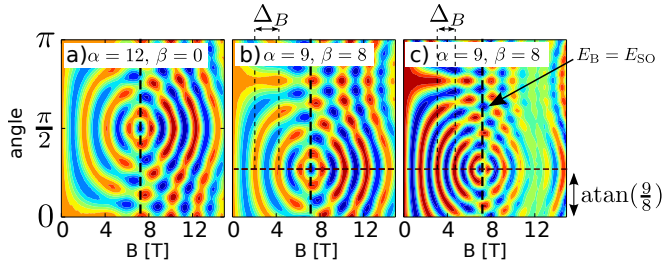


Figure 3. a) The conductance image (arbitrary units) obtained with simple model for electron source located at $(x, y) = (-1500\text{nm}, 0\text{nm})$ as a function of magnetic field direction and amplitude with only Rashba interaction present in the Hamiltonian. b) Same as a) but with Rashba and Dresselhaus SO interactions present. c) Same as b) but with the source located at position $(-2000\text{nm}, 0\text{nm})$. The values of the coupling constants α and β are given in $\text{meV} \times \text{nm}$ units. The vertical dashed line indicate $B = 7.2$ T for which the Zeeman energy is equal to the SO coupling energy, $E_B = E_{SO}$, see text. The horizontal dashed line shows the angle $\arctan\left(\frac{\alpha}{\beta}\right)$.

The results of Fig. 3 contain a distinct circular pattern in the θ, B plane. The angular coordinate of the center of the pattern is exactly $\theta = \arctan\left(\frac{\alpha}{\beta}\right)$, which thus allows one to determine the ratio of the Rashba and Dresselhaus constants. The effective SO coupling con-

stant $\gamma_{\text{eff}} = \sqrt{\alpha^2 + \beta^2}$ can be read-out from the the position of the center of the pattern on the B scale. The position is given by the condition: $E_B = E_{SO}$, or $\frac{1}{2}g\mu_B B = k_F \gamma_{\text{eff}}$, given that the Fermi wave vector is known. In general, when the SO coupling and / or the Zeeman effect is present the Fermi wave vector for 2DEG is spin dependent [21]. However, for the condition $E_B = E_{SO}$ the off-diagonal terms of the Hamiltonian (2) vanish and the Fermi wavevector is directly related to the Fermi energy $E_F = \frac{\hbar^2 k_F^2}{2m_{\text{eff}}}$, which for the adopted parameters gives $k_F = 0.156/\text{nm}$. For $\gamma_{\text{eff}} = 12$ meV nm one obtains $E_{SO} = 1.875$ meV, which agrees with $E_B = \frac{1}{2}g\mu_B B$ for $B = 7.2$ T – as indicated by the center of the pattern in Fig. 3. In an experimental situation the value of γ_{eff} could be extracted from the B coordinate of the center of the pattern, as

$$\gamma_{\text{eff}} \approx \frac{g\mu_B B}{2k_F}.$$

Let us now comment on the period of the oscillations visible in Fig. 3. In Figure 3(c) one notices a reduction of the period with respect to 3(b) with the source-impurity distance increased to 2000 nm from 1500 nm. The period of the oscillations Δ_B is $\Delta_B^{(c)} \approx 1.5\text{T}$ in (c), and $\Delta_B^{(b)} \approx 2.0\text{T}$ in (b). The ratio $\Delta_B^{(c)}/\Delta_B^{(b)} \approx 3/4$, is exactly an inverse of the source-impurity d_{s-i} distance ratio $2000/1500 = 4/3$. Indeed both Δ_B and the d_{s-i} are related. The electron density between the source and the impurity can be expressed as a superposition of standing waves with (in general) four different frequencies $k_i = \{k_+^+ + k_+^-, k_+^+ + k_-^-, k_-^+ + k_+^-, k_-^+ + k_-^-\}$, which occur as superpositions of the Fermi wave vectors k_σ^\pm

$$\rho = \sum_\sigma \langle \Psi_\sigma | \Psi_\sigma \rangle = \sum_{i=1}^4 c_i \cos(k_i(\mathbf{B}) d_{s-i}).$$

Quantum transport calculations. After the intuitions gained by the approximate analytical model of the previous section we move to a fully-fledged calculations of the coherent charge transport using a standard numerical method described in detail in Ref. [35]. The method [35] is based on the quantum transmitting boundary solution of the quantum scattering equation at the Fermi level implemented in the finite difference approach, which produces the electron transfer probability used in the Landauer formula for conductance summed over the subbands of the channels far from the scattering area. Zero temperature is assumed.

For the numerical calculations we consider a channel extended along the x direction, hence k_x in Eq. (2) remains a quantum number characterizing the asymptotic states of the channel. Within the computational box the wave vector is replaced by an operator $\mathbf{k} = (k_x, k_y) = -i\nabla$. The effects described in the previous section dealt with interference of the electron waves between the source

and the impurity. In fact, the role of the source can be played by any scattering center, and the extraction of the SO coupling constant requires a presence of two or more scatterers.

We consider a channel of width W , which carries M transport modes at the Fermi level. In Fig. 4(d) we presented the conductance results for a clean channel of width $W = 180\text{nm}$ and the computational box of length $L = 1.6\mu\text{m}$. A smooth potential barrier is introduced across the channel with height 10 meV and width 200nm . Depending on the orientation of the magnetic field the number of transport modes varies between $M = 17$ and $M = 18$. The simulation was performed for $\alpha = 9\text{meVnm}$ and $\beta = 8\text{meVnm}$ as in Fig. 3(b,c). The conductance plot possesses an extremum precisely at the angle of $\theta = \arctan \frac{9}{8}$. The magnetic field of the extremum is slightly shifted to lower values than 7.2 T – which is a result of the reduction of k_x within the potential barrier. The lack of conductance oscillations that were observed above in Fig. 3 results from a small barrier length ($d_{s-i}=200\text{nm}$).

The oscillations reappear when one takes into account a random disorder without the short potential barrier. Figure 4(c) displays the conductance for the channel of the same width and length. The potential – displayed in Fig. 4(a) is locally varied within the range of $(-0.5E_F, 0.5E_F)$. The perturbation induces a multitude of scattering evens – the local density of states at the Fermi level for $B = 0$ is displayed in Fig. 4(b). In spite of the complexity of the density of states the angular shift is still $\arctan(9/8) \approx \pi/4$. The shift of the G extremum along the B scale with respect to 7.2 T is detectable – but small and of an opposite sign than in Fig. 4(d). This shift is related to the fact that for a finite width channel one cannot simply attribute a zero value to k_y , and k_y is an operator mixing the subbands. These – small but detectable – effects of a finite W disappear completely for a wider channel – which is illustrated in Fig. 4(e) for $W = 0.8\mu\text{m}$. Here, the number of conducting bands varies between 80 and 81. The local extremum of conductance appears exactly at the positions indicated in the previous section. Note, that although the number of subbands change by 1 in Fig. 4(c,e), the variation of conductance is as large as $\sim 3e^2/h$ in Fig. 4(c) and $\sim 6e^2/h$ in Fig. 4(e). For completeness in Fig. 4(f) we presented calculations for a twice smaller SO coupling constants $\alpha = 4.5\text{ meVnm}$, $\beta = 4\text{ meVnm}$, and $\gamma_{\text{eff}} = 6\text{meVnm}$. The position of the maximal G along the B scale is consistently reduced from 7.2 T to 3.6 T , and the orientation of the magnetic field vector corresponding to the extremum is unchanged.

Summary. We have shown that the in-plane magnetic field can lift the off-diagonal terms of the transport Hamiltonian for the two-dimensional electron gas that result from the Zeeman effect and the SO interaction. The effect appears only for a precisely chosen value and orientation of the external magnetic field, and excludes the

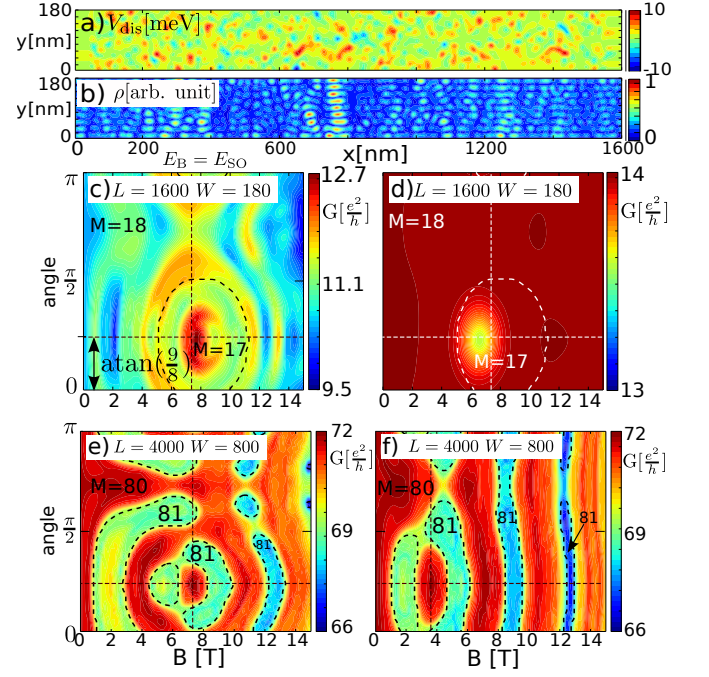


Figure 4. a) Potential disorder in simulated quantum wire. b) Local density of states obtained for channel from (a) at $B=0$. c) Conductance through the wire in (a) as a function of magnetic field amplitude B and direction $angle$. d) Same as c) but with one potential barrier in the middle of channel instead of random disorder. e) Same as (c) but for the wire with length $L = 4000\text{nm}$ and $W = 800\text{nm}$. f) Same as (e) but for SO couplings twice smaller $\gamma_{\text{eff}} = 6\text{meVnm}$. For comparison of (c,e) see Fig. 3(b). The values M show the number of non-degenerated modes in the channel.

spin mixing effects that accompany the backscattering in presence of the SO coupling. In consequence the conductance maps for a system containing two or more scatterers – intentionally introduced – or inherently present in a disordered sample exhibit a pronounced extremum as a function of the magnetic field modulus B and orientation θ . An experimental value of B – for which the Zeeman energy is equal to the SO coupling energy – should allow one to extract the effective SO coupling constant including both the Rashba and Dresselhaus terms $\gamma_{\text{eff}} = \sqrt{\alpha^2 + \beta^2}$. The orientation of the in-plane magnetic field θ for the extremum is equal to $\theta = \arctan \left(\frac{\alpha}{\beta} \right)$. Thus, a mere two-terminal measurement of the conductance of the system in a rotated external magnetic field should allow for an experimental determination of both linear SO coupling constants. .

Acknowledgments This work was supported by National Science Centre according to decision DEC-2015/17/N/ST3/02266, and by PL-Grid Infrastructure. The first author is supported by the scholarship of Krakow Smoluchowski Scientific Consortium from the funding for National Leading Research Centre by Ministry of Science and Higher Education (Poland) and by

the Etiuda stipend of the National Science Centre (NCN) according to decision DEC-2015/16/T/ST3/00310.

-
- [1] A. Manchon, H. C. Koo, J. Nitta, S. M. Frolov, and D. R. A., Nat. Mater. **14**, 871 (2015)
 - [2] Y. Ohno, R. Terauchi, T. Adachi, F. Matsukura, and H. Ohno, Phys. Rev. Lett. **83**, 4196 (1999)
 - [3] M. I. D'yakonov and V. I. Perel, JETP Lett. **13**, 467 (1971)
 - [4] J. Kainz, U. Rössler, and R. Winkler, Phys. Rev. B **70**, 195322 (2004)
 - [5] J. E. Hirsch, Phys. Rev. Lett. **83**, 1834 (1999)
 - [6] J. Sinova, D. Culcer, Q. Niu, N. A. Sinitsyn, T. Jungwirth, and A. H. MacDonald, Phys. Rev. Lett. **92**, 126603 (2004)
 - [7] Y. K. Kato, R. C. Myers, A. C. Gossard, and D. Awschalom, Science **1910**, 306 (2004)
 - [8] M. Koenig, S. Wiedmann, C. Bruene, A. Roth, H. Buhmann, L. W. Molenkamp, X.-L. Qi, and Z. S.-C., Science **318**, 766 (2007)
 - [9] B. A. Bernevig, J. Orenstein, and S.-C. Zhang, Phys. Rev. Lett. **97**, 236601 (2006)
 - [10] J. D. Koralek, C. P. Weber, J. Orenstein, B. A. Bernevig, S.-C. Zhang, S. Mack, and D. D. Awschalom, Nature **458**, 610 (2009)
 - [11] M. P. Walser, C. Reichl, W. Wegscheider, and G. Salis, Nature Phys. **8**, 757 (2012)
 - [12] V. Mourik, K. Zuo, S. M. Frolov, S. R. Plissard, E. P. A. M. Bakkers, and L. P. Kouwenhoven, Science **336**, 1003 (2012)
 - [13] P. Debray, S. M. S. Rahman, J. Wan, R. S. Newrock, M. Cahay, A. T. Ngo, S. E. Ulloa, S. T. Herbert, M. Muhammad, and J. M., Nature Nanotech. **4**, 759 (2009)
 - [14] S. Datta and B. Das, Appl. Phys. Lett. **56**, 665 (1990)
 - [15] J. Schliemann, J. C. Egues, and D. Loss, Phys. Rev. Lett. **90**, 146801 (2003)
 - [16] I. Žutić, J. Fabian, and S. Das Sarma, Rev. Mod. Phys. **76**, 323 (2004)
 - [17] P. Chuang, S.-C. Ho, L. W. Smith, F. Sfigakis, M. Pepper, C.-H. Chen, J.-C. Fan, J. P. Griffiths, I. Farrer, H. E. Beere, G. A. C. Jones, D. A. Ritchie, and T.-M. Chen, Nat Nano **10**, 35 (2015)
 - [18] S. Bednarek and B. Szafran, Phys. Rev. Lett. **101**, 216805 (2008)
 - [19] L. Meier, G. Salis, I. Shorubalko, E. Gini, S. Schoen, and K. Ensslin, Nature Phys. **3** (2007)
 - [20] Y. Bychkov and E. Rashba, J. Phys. C **17**, 6039 (1984)
 - [21] R. Winkler, *Spin-orbit Coupling Effects in Two-Dimensional Electron and Hole Systems* (Springer-Verlag Berlin Heidelberg, 2003)
 - [22] J. Nitta, T. Akazaki, H. Takayanagi, and T. Enoki, Phys. Rev. Lett. **78**, 1335 (1997)
 - [23] G. Engels, J. Lange, T. Schäpers, and H. Lüth, Phys. Rev. B **55**, R1958 (1997)
 - [24] I. Lo, J. K. Tsai, W. J. Yao, P. C. Ho, L. W. Tu, T. C. Chang, S. Elhamri, W. C. Mitchel, K. Y. Hsieh, J. H. Huang, H. L. Huang, , and W.-C. Tsai, Phys. Rev. B **65**, R161306 (2002)
 - [25] J. H. Kwon, H. C. Koo, J. Chang, S.-H. Han, and J. Eom, Appl. Phys. Lett. **90**, 112505 (2007)
 - [26] D. Grundler, Phys. Rev. Lett. **84**, 6074 (2000)
 - [27] K.-H. Kim, H.-j. Kim, H. C. Koo, J. Chang, and S.-H. Han, Appl. Phys. Lett. **97**, 012504 (2010)
 - [28] B. Das, D. C. Miller, S. Datta, R. Reifengerger, W. P. Hong, P. K. Bhattacharya, J. Singh, and M. Jaffe, Phys. Rev. B **39**, 1411 (1989)
 - [29] Y. Ho Park, H.-j. Kim, J. Chang, S. Hee Han, J. Eom, H.-J. Choi, and H. Cheol Koo, Appl. Phys. Lett. **103**, 252407 (2013)
 - [30] T. Koga, J. Nitta, T. Akazaki, and H. Takayanagi, Phys. Rev. Lett. **89**, 046801 (2002)
 - [31] S. D. Ganichev, V. V. Bel'kov, L. E. Golub, E. L. Ivchenko, P. Schneider, S. Giglberger, J. Eroms, J. De Boeck, G. Borghs, W. Wegscheider, D. Weiss, and W. Prettl, Phys. Rev. Lett. **92**, 256601 (2004)
 - [32] L. Meier, G. Salis, I. Shorubalko, E. Gini, S. Schon, and K. Ensslin, Nature Phys. **3**, 650 (2007)
 - [33] E. A. de Andrada e Silva, G. La Rocca, and F. Bassani, Phys. Rev. B **55**, 16293 (1997)
 - [34] K. Kolasiński, B. Szafran, and M. P. Nowak, Phys. Rev. B **90**, 165303 (2014)
 - [35] K. Kolasiński, A. Mreńca-Kolasińska, and B. Szafran, Phys. Rev. B **93**, 035304 (2016)